Research Article

Johannes Störkle, Luzia Hahn and Peter Eberhard*

Simulation of segmented mirrors with adaptive optics

https://doi.org/10.1515/aot-2018-0063
Received November 29, 2018; accepted January 29, 2019; previously published online February 23, 2019

Abstract: This work deals with the simulation-based investigation and control of optical systems that are mechanically influenced. Here, the focus is on the dynamic-optical modeling of vibration-sensitive, segmented mirror systems, which are used, for example, in large astronomic telescopes. Furthermore, an adaptive optical unit usually compensates for the optical aberrations due to atmospheric disturbances. In practice, these aberrations are detected and corrected within a few seconds using deformable mirrors. However, to further improve the performance of these optical systems, dynamic disturbances in the mechanics, i.e. small movements and deformations of the optical surfaces, must also be taken into account. For the investigation of such cases, multidisciplinary simulation methods are developed and presented.

Keywords: adaptive optics; mechanical-dynamic simulation; segmented mirror.

1 Introduction

According to the concept of adaptive optics (AO), a deformable mirror is used to compensate the optical aberrations due to atmospheric disturbances. The atmospheric disturbances are usually in the low-frequency range, and it is sufficient to use sample times of a couple of seconds. Thereby, the related optical aberrations are typically detected using a Shack-Hartmann wavefront sensor [1]. The task of the AO unit is to control the deformation of an elastic mirror such that the current aberration is compensated. This ensures an undisturbed space observation or perfect image exposure. As sketched in Figure 1A, the elastic M2 compensates the low-frequency atmospheric turbulences with the use of a controlled low-frequency deformation.

However, the lightweight structures of a telescope mirror are also sensitive to deformations and dynamic disturbances. During astronomical observation, e.g. dynamic wind loads, the AO unit or other motion systems can unintentionally excite the whole system including mounted mirrors. The mechanical disturbances can cause vibrations of the optical elements, which are typically in the range of one up to several hundred hertz. Even if the atmospheric disturbances are not taken into account, aberrations due to the mechanical disturbances occur, as indicated in Figure 1B. To compensate for the mechanical vibrations, they can be detected in real-time, e.g. using laser Doppler vibrometers, multiple position or acceleration sensors, and strain gauges, or they can be estimated by a model-based state observer. Based on this, the reconstruction of the mechanical mirror deformation can be performed (see also Refs. [2, 3]). Thus, the resulting high-frequency optical aberrations can be compensated with a controlled high-frequency deformation of the second mirror. This approach is depicted in Figure 1C. In the presence of delays, advanced feed-forward and feedback control techniques can be used as proposed in Refs. [4, 5]. With the use of a superposition of the correcting deformations of the low-frequency atmospheric and high-frequency mechanical aberrations, the deformable secondary mirror can be controlled to achieve a compensation of the high- and low-frequency aberrations at the same instant time.

Apparently, dynamic-optical analyses with integrated modeling and simulation, as described in Refs. [6, 7], are required for such developments. In the following, an application is presented, where an integrated model is used to perform dynamic analyses of a optical system. Atmospheric disturbances are not taken into account, but mechanical deformations are considered.

***Corresponding author: Peter Eberhard,** Institute of Engineering and Computational Mechanics, University of Stuttgart, Pfaffenwaldring 9, 70569 Stuttgart, Germany,
e-mail: peter.eberhard@itm.uni-stuttgart.de.
https://orcid.org/0000-0003-1809-4407
Johannes Störkle and Luzia Hahn: Institute of Engineering and Computational Mechanics, University of Stuttgart, Pfaffenwaldring 9, 70569 Stuttgart, Germany

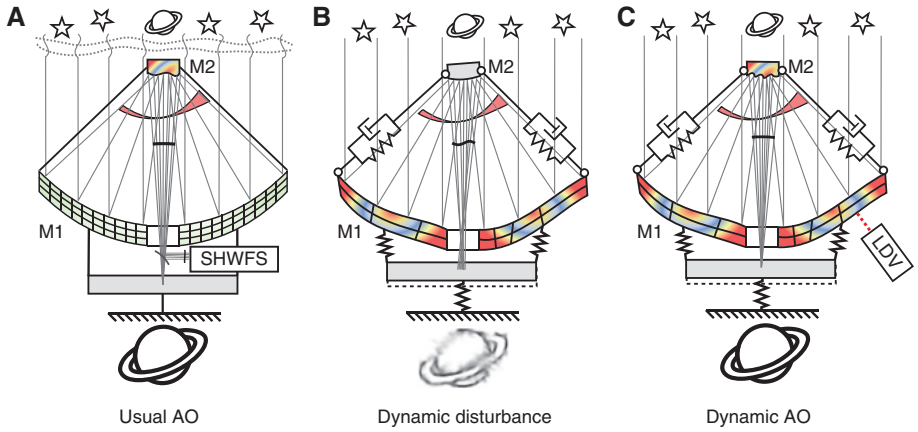

Figure 1: Sketches of AO consisting of two mirrors. M1 is annular and M2 is circular. Atmospheric disturbances are only considered in (A); the resulting aberrations are corrected with a controlled deformation of M2. The shown deformations of M1 in (B and C) are sketched dynamic elastic mirror deformations and the resulting aberrations are corrected in (C) with the controlled deformation of M2.

2 Ray tracing for segmented mirrors

One of the most important challenges during a dynamic-optical simulation is the handling and preprocessing of the interface data, which have to be transformed from the mechanical to the optical model. Thereby, the surface kinematics and the polynomial approximation are substantial tasks that are explained in Refs. [8, 9].

To simulate the ray optical behavior of a segmented mirror, the typical sequential ray tracing has to be adjusted. On the one hand, the rays have to be assigned to the different segments that are usually next to each other; on the other hand, the computation should be as efficient as possible. Therefore, the algorithm contains a coarse search based on the reference surface in the undisturbed 'reference configuration' and a subsequent fine search. The latter is used for the computation of the real reflection at the disturbed segments in the 'current configuration'. Thereby, the surface of the deformed segments is the sum of the continuous undeformed surface description $z_{\text{ref}}(x, y)$ and the approximation of the node displacements with the use of Zernike polynomials:

$$z_{\text{deform}}(x, y) = \sum_j c_j Z_j(x, y), \tag{1}$$

See also Refs. [7, 8]. The ray tracing procedure for segmented mirrors is illustrated in Figure 2, where a specific segment is considered.

The detailed ray tracing steps can be formulated as follows:

(a) Compute intersection points of all rays with the reference surface S_{ref}.
(b) Loop through all segments with the following substeps:
(c) Select the ray candidates of the related intersection points within a quadratic area of interest in the neighborhood of the considered segment (coarse search).
(d) Transform 'all' rays into the surface system S_i of the considered segment, whereby the rigid-body translation $\Delta \boldsymbol{s}_i$ and rotation $\Delta \boldsymbol{R}_i$ are also taken into account.
(e) Compute the actual intersection points of the ray candidates with the moved and deformed surface, which belongs to the considered segment (fine search).
(f) Obtain the corner points of the considered segment in the 'current configuration', which could be distorted due to surface deformation.
(g) Select the actual intersection points within the distorted hexagon shape.
(h) Store the indices, coordinates, directions, and normal vectors of the resulting rays, which can be assigned to the considered segment.
(i) Remove all rays that are not assigned to a segment.
(j) Calculate the new directions of all remaining rays according to the reflection law using the incident ray directions and the normal vectors.
(k) As the final intersection points and new direction vectors of all outgoing rays are presented with respect to the last segmented surface, the usual sequential ray tracing can be continued.

3 AO for a segmented telescope

The dynamic-optical simulation model represents the AO control of a mechanically disturbed telescope. Thereby,

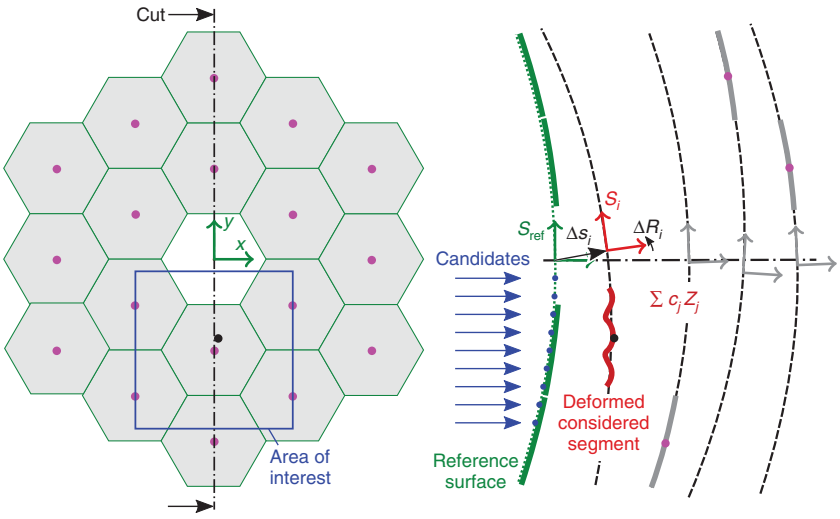

Figure 2: Overview of the ray tracing at a disturbed segmented mirror. In particular, the considered segment with the surface S_i is not only deformed but also has a rigid-body motion. The right-hand side shows the marked cut of the segmented mirror in the tangential view.

the model parameters of the Thirty Meter Telescope (TMT) construction proposal according to Ref. [10] are used, which describe a typical astronomical ground-based telescope. For the following investigation, visible light with a wavelength of $\lambda = 550$ nm is taken into account. First, the kinematic-optical model is explained. Second, the design of the controller for the optical compensation is derived. Finally, the simulation results for a single-field point clarify the functionality.

3.1 Kinematic-optical model under disturbance

The TMT consists of a segmented primary mirror (M1) with a global diameter of 30 m, a deformable secondary mirror (M2), and a planar tertiary mirror (M3). A sketch of the optical model and a visualization of the optical surfaces are introduced in Figure 3. As M2 stops the incident rays at the center region of the field, the optical system is obscured, such that M1 has an annular shape.

In particular, M3 is rotated with an angle of 45° with respect to the *y*-axis. For the construction, it is proposed to realize M1 with 492 mirror segments. However, to demonstrate the simulation-based control of M2 at lower computational cost, the system is simplified here to just 18 segments. On an ordinary computer, the dynamic-optical simulation of the resulting model has computation times in the several minutes range.

The considered simplified telescope system is illustrated in Figure 4A, where the sixth segment is marked. It is further assumed that only the segments of M1 are

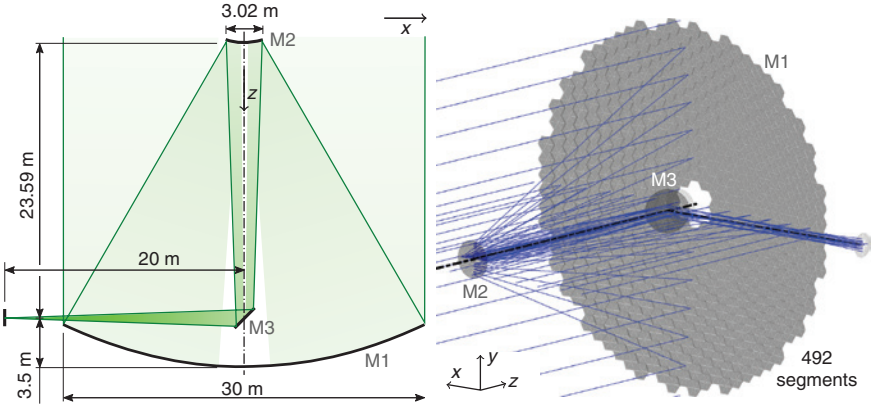

Figure 3: Sketch and visualization of the optical model of the TMT.

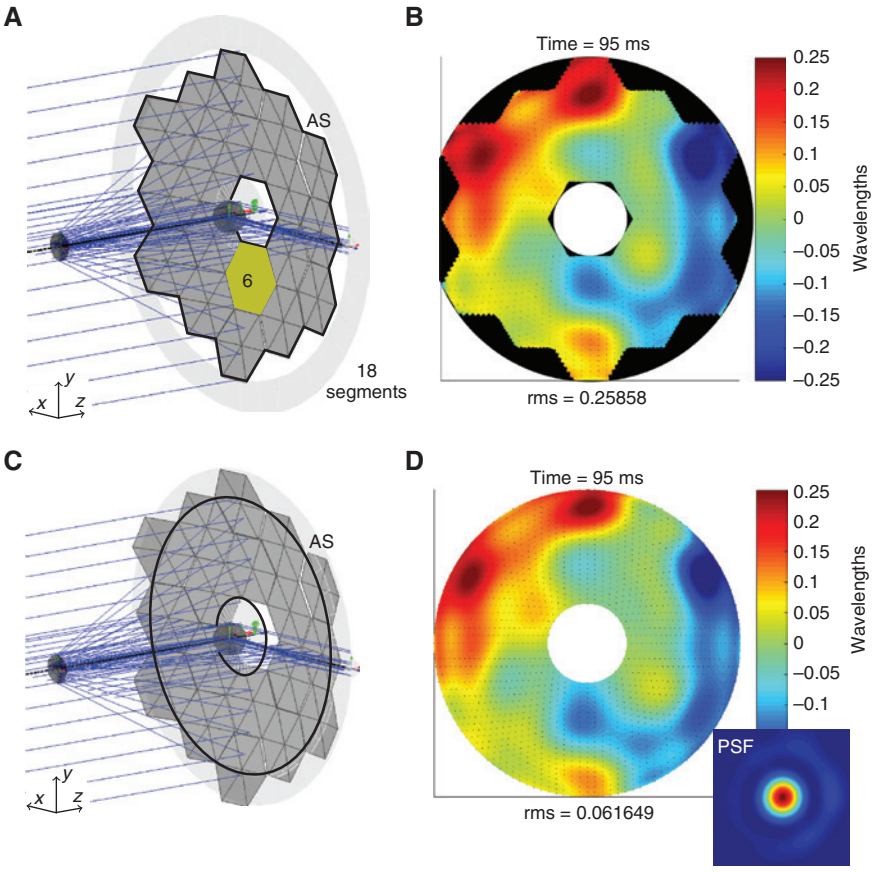

Figure 4: Visualization of the two different kinmatic-optical models with 18 segments. The actual telescope with the cornered pupil is illustrated in (A) and the related WFA with undefined regions is depicted in (B), whereby the RMS results inaccurately. In contrast, the simplified optical model with a circular pupil is shown in (C). The WFA and the correct RMS are presented in (D).

mechanically disturbed in the z-direction. Each segment is subject to a predefined movement that results in a maximal segment translation of $\pm\Delta s_z \approx 70$ nm. Thereby, the optical system remains diffraction limited. The corresponding motions of the individual segments indicated by their numbers are illustrated in Figure 5 for a considered simulation duration of 100 ms. With a second model, the influence of the deformation of the sixth segment is simulated, whereby the related values are in the same range.

Anyway, the actual optical system and the related wavefront aberration (WFA) are shown at the simulated time $t = 95$ ms in Figure 4A and B. Thereby, it is assumed that the inner and outer incident rays are stopped according to the cornered shape of the segmented mirror. As a result, the aperture stop (AS), the entrance pupil, and the exit pupil are also edgy. On the right-hand side, the colors represent the accuracy of the optical system with respect to the z-translations of the segments. According to Ref. [8],

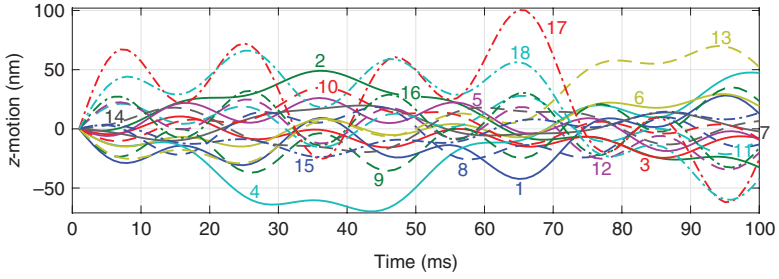

Figure 5: Rigid-body motion of M1 segments due to the mechanical disturbances.

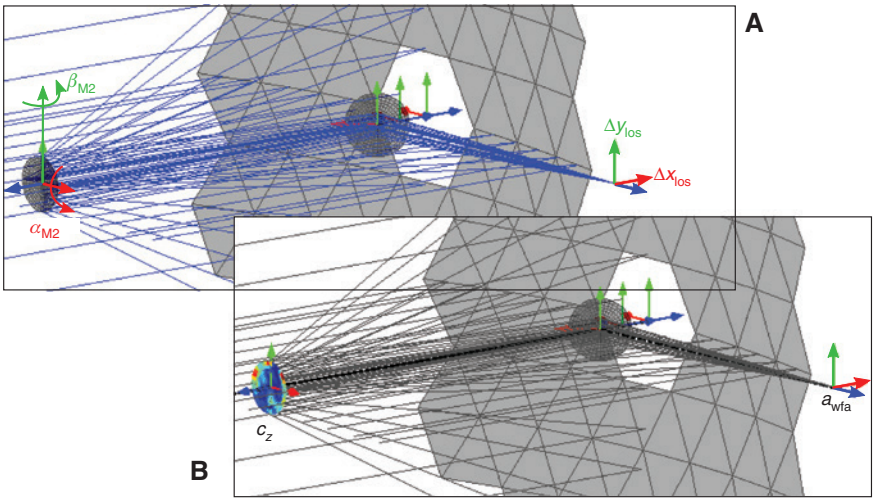

Figure 6: Strategy for the optical compensation by means of either a rigid (A) or a deformable (B) M2.

if the mirror is circular, for the WFA, the value ΔW can be approximated using the root mean square (RMS) value of the n_j Zernike standard polynomial coefficients c_j:

$$\Delta W_{\text{rms}} = \sqrt{\sum_{j=4}^{n_j} c_j^2}. \tag{2}$$

However, as the mirror is annular, annular Zernike polynomials must be used for the WFA approximation [11]. Consequently, there are some undefined regions next to the outer and inner segment bounds. Thus, the resulting polynomial coefficients c_j and the related RMS value are not representative for the actual aberration. At least, the influence of the segment translations on the WFA is correctly visualized within the segments.

In contrast, Figure 4C and D depicts for comparison the system with an annular AS. The remaining rays are uniformly distributed on the whole annular pupil within the segmented area. Hence, the approximated Zernike polynomials perfectly describe the WFA through their coefficients, and this annular model is considered in the following during the controller design. In the point-spread function plot on the lower right-hand side, one can also see the distinct outer ring due to the annular pupil shape.

3.2 Control strategy for M2

As introduced, the strategy during AO is to compensate for optical aberrations actively using a controllable mirror. For the regarded telescope, two different approaches are investigated for the control of M2 as illustrated in Figure 6.

On the one hand, the line of sight (LOS) aberration due to the disturbed M1 can be corrected by means of a target rigid-body motion of M2. Thus, a rotation around the x- and y-axes can be applied with angles α_{M2} and β_{M2}, as indicated in Figure 6A. This change results in the LOS displacements Δx_{los} and Δy_{los} on the image plane and the sensitivity analysis can be performed. According to Ref. [8], the corresponding matrix of the kinematic-optical sensitivities can be computed, e.g. with $h = 1\text{e-}6$ rad ≈0.2 arcsec. This leads to

$$\underbrace{\begin{bmatrix}\Delta x_{los}\\ \Delta y_{los}\end{bmatrix}}_{\Delta \boldsymbol{a}_{los}} = \underbrace{\begin{bmatrix}-2.4945\text{e}-5 & -85460\\ 85460 & 1.7364\text{e}-5\end{bmatrix}}_{\boldsymbol{C}_{a,r,los}} \cdot \underbrace{\begin{bmatrix}\alpha_{M2}\\ \beta_{M2}\end{bmatrix}}_{\boldsymbol{q}_{r,M2}}, \tag{3}$$

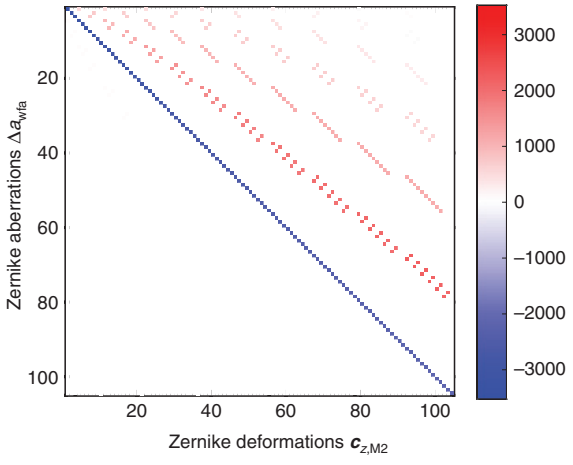

Figure 7: Matrix of kinematic-optical sensitivities $C_{a,e,wfa}$, for a deformable M2.

where the rigid-body motions are collected in the vector $\boldsymbol{q}_{\mathrm{r,M2}}$. To compensate the occurring LOS motion $\boldsymbol{a}_{\mathrm{los}}(t)$ during a disturbance, the target motion of M2 can be calculated by means of the rearrangement:

$$\boldsymbol{q}_{\mathrm{r,M2,target}}(t) = -\boldsymbol{C}_{a,\mathrm{r,los}}^{-1} \cdot \boldsymbol{a}_{\mathrm{los}}(t). \tag{4}$$

On the other hand, the general WFA described by 105 Zernike coefficients can be corrected by means of an appropriate target deformation of M2. As indicated in Figure 6B, one can investigate the influence of M2 deformation $\boldsymbol{c}_{\mathrm{z,M2}}$, which is also described by 105 Zernike coefficients, on the WFA. The latter is denoted with $\Delta\boldsymbol{a}_{\mathrm{wfa}}$. In analogy to the upper case, the matrix of kinematic-optical sensitivities $\boldsymbol{C}_{\mathrm{a,e,wfa}}$ for the individual coefficients describing a Zernike deformation can be computed, e.g. with $h = 1\mathrm{e}\text{-}5$ mm. This can be formulated with

$$\underbrace{\begin{bmatrix} \vdots \\ c_j \\ \vdots \end{bmatrix}}_{\Delta\boldsymbol{a}_{\mathrm{wfa}}} = \boldsymbol{C}_{a,\mathrm{e,wfa}} \cdot \underbrace{\begin{bmatrix} \vdots \\ c_{j,z,\mathrm{M2}} \\ \vdots \end{bmatrix}}_{\boldsymbol{c}_{z,\mathrm{M2}}}. \tag{5}$$

The resulting matrix structure is visualized in Figure 7. Obviously, the fully occupied diagonal entries clarify a strong relation between a Zernike deformation coefficient and a Zernike aberration coefficient of the same type. In addition, for most of the Zernike deformations, there are small dependencies at lower orders of optical aberrations

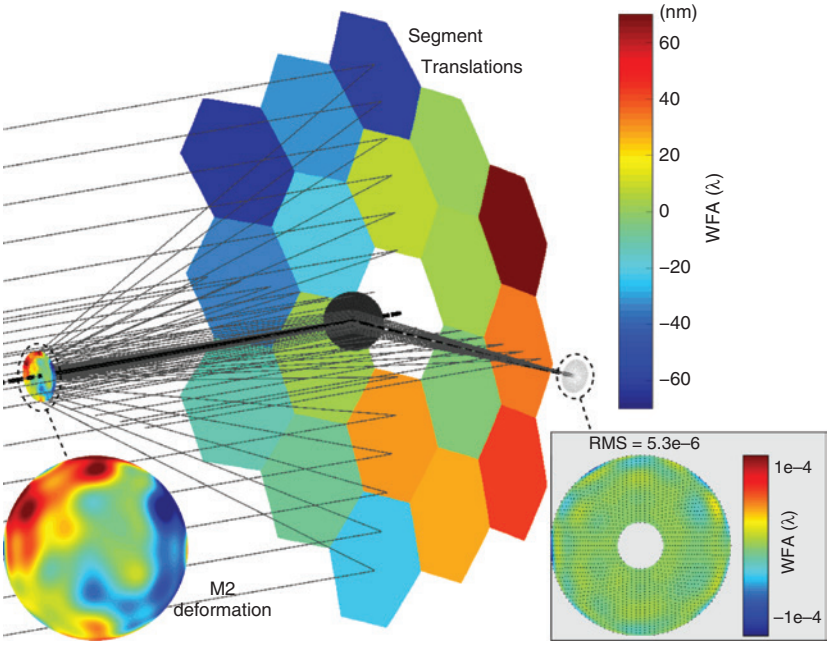

Figure 8: Visualization of the displacements of M1 segments, the correcting M2 deformation, and the nearly vanishing optical aberrations at $t = 95$ ms.

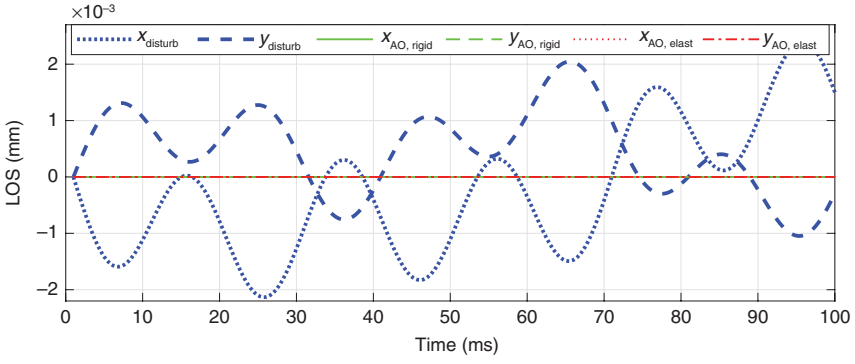

Figure 9: Simulated LOS for the different models.

probably due to the nonlinear projection of the optical rays.

To compensate the occurring WFA denoted with $\boldsymbol{a}_{\text{wfa}}(t)$ during a disturbance, the target deformation of M2 can be calculated through the rearrangement:

$$\boldsymbol{c}_{z,\text{M2,target}}(t) = -\boldsymbol{C}_{a,\text{e,wfa}}^{-1} \cdot \boldsymbol{a}_{\text{wfa}}(t). \tag{6}$$

Next, the control strategies are tested within the simulation model.

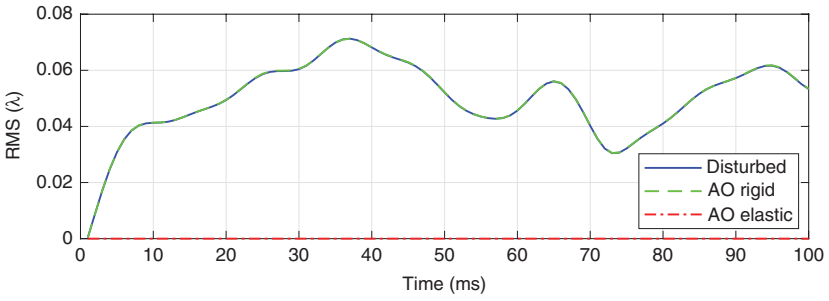

Figure 10: Simulated RMS for the different models.

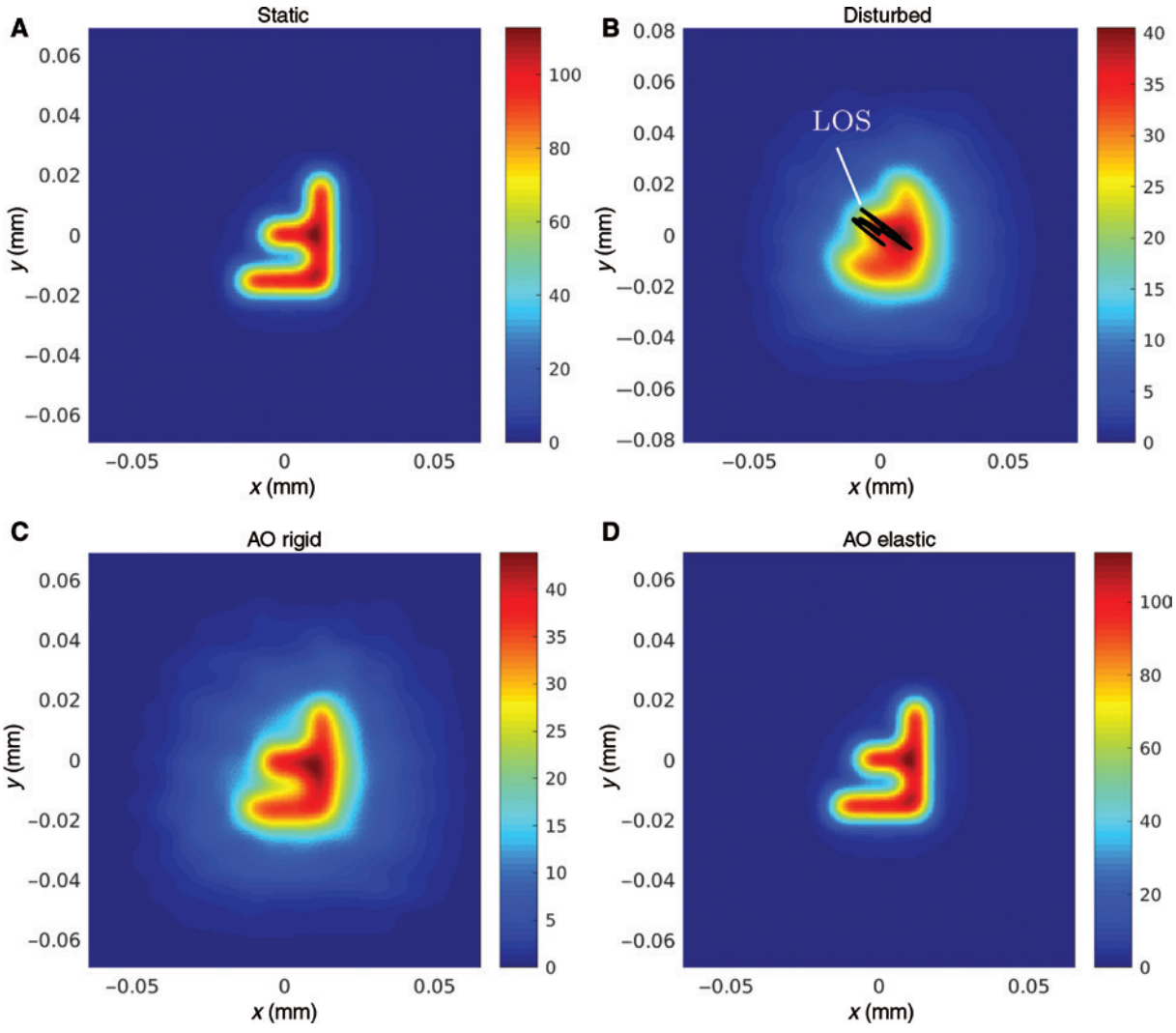

Figure 11: Resulting images of the different models after an exposure duration of 100 ms.

3.3 Simulation of the AO control

The derived compensation approaches are finally investigated using the considered kinematic-optical simulation model. Thereby, the aberrations of the uncontrolled system can be simulated in a preprocessing step, and the target M2 motion and deformation are executed during the actual AO simulation.

Figure 8 shows the AO simulation results at $t = 95$ ms. At this time instant, the segments of M1 are displaced with about ±70 nm, which is indicated by the corresponding colors. For the optical compensation, it is required to deform M2 according to the color distribution of the lower left-hand side, whereby the values are also in the same order of magnitude. One can also see according to the colors that the shape of the deformation is the contrary of the segment displacements. In the box on the lower right-hand side, the resulting WFA is visualized, which is computed by means of 2000 rays, and it is quite small in the whole region. This is also represented by the vanishingly small RMS value. Thus, the design AO control works very well within the simulation. The higher the number of rays is and the more Zernike are used for the WFA fit, the better one can calculate the actual WFA and the target M2 deformation for the AO. Of course, there are also numerical limitations and numerical noise issues can occur due to the least-squares fitting, so one always has to find a good compromise; here, a quite low number of rays has turned out to be sufficient [8]. For practical applications, there are usually some inaccuracies and latencies due to the internal dynamics of the sensing and actuating systems, which also have to be taken into account.

To assess the AO performance during the complete simulation duration, the varying LOS of the different models are considered according to Figure 9. Obviously, the initial disturbed motions $x_{\text{disturbed}}$ and $y_{\text{disturbed}}$ are perfectly corrected for both AO approaches, the first with the tilts of a rigid M2 according to Equation (4) and the second with a deformation of an elastic M2 of Equation (6).

However, the corresponding RMS values of the WFA with respect to the simulation time are drawn in Figure 10. As expected, the values of the rigid AO are not decreased in comparison to the uncontrolled and fully disturbed results, as the corrected tilts are not considered within the RMS; see also Equation (2). Anyway, the elastic AO method optimally compensates the remaining RMS.

The WFA of the ray tracing rates an optical system quantitatively. Additionally, a wave-optical consideration by means of image and exposure simulations allows for a qualitative assessment of an optical system. Thereby, effects such as refraction or interference are considered using Fourier optics. For instance, one can project an object with the shape of the letter 'F' onto the image plane to assess the quality of the irradiance map. The resulting images of this exposure simulation of the static and disturbed systems are presented

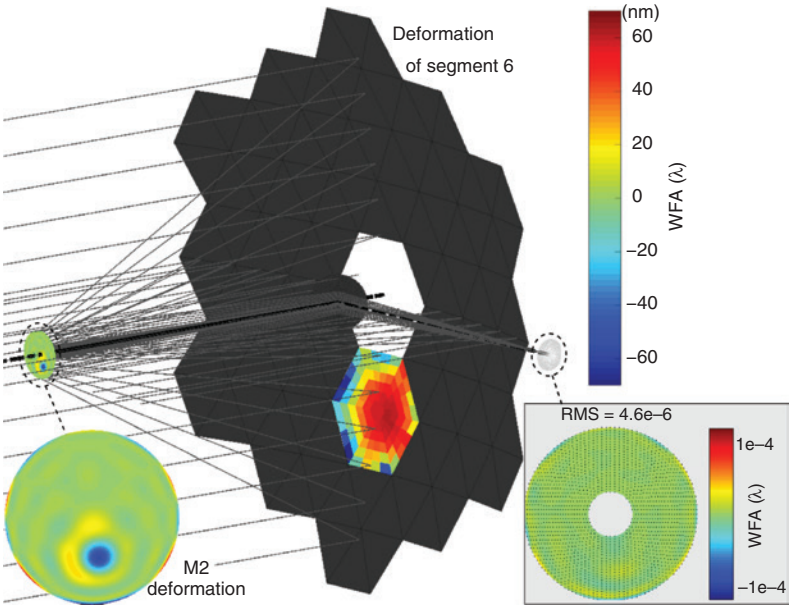

Figure 12: Visualization of the deformation of the sixth segment of M1, the correcting M2 deformation, and the vanishing optical aberrations at $t = 95$ ms.

in Figure 11A and B. The disturbance is scaled for the visualization by a factor of 5, such that the shape of the LOS and the other optical aberrations are clarified. The models with the rigid- and elastic-controlled M2 are shown in Figure 11C and D. On the one hand, the rigid AO model yields an improved image; on the other hand, the elastic AO model leads to a perfect result, which is almost identical to the static case.

Finally, the investigation can be extended to the consideration of possible elastic segment deformations that could occur due to mechanical disturbances [12]. Figure 12 briefly illustrates that the proposed AO compensation concepts are also applicable. The local aberration due to the disturbed segment is corrected by means of a local deformation of M2 and the resulting WFA is perfectly eliminated.

4 Conclusion

Astronomical telescopes are based on cutting-edge technologies, which are developed at the limits of physical feasibility. Due to rising requirements for accuracy and resolution, these optical systems are also sensitive to mechanical disturbances. Thereby, it is the difficulty to switch from the mechanical and optical domain, to analyze segmented mirror systems, and to design the related control efficiently. For instance, if a surface or segment is moving, the motion has to be passed to the ray tracing algorithm in a relative description. In addition, if there are deformable optical elements in the mechanical model, the related surfaces have to be translated to a continuous surface description, as a sequential ray tracing is used for the optical analyses. As an example, the development of an adaptive optical controller for an astronomical telescope was presented. The kinematic-optical model with a segmented primary mirror was simulated under disturbances. In addition, a control strategy for the deformable secondary mirror was designed, tested, and simulated for different load cases.

All shown mechanical-optical simulations have been performed using the Matlab-based code OM-SIM[1] developed at the Institute of Engineering and Computational Mechanics at the University of Stuttgart.

Acknowledgments: The authors thank Alois Herkommer (Institute of Applied Optics, University of Stuttgart) for the invitation to participate in this special issue.

References

[1] H. Ebel, Modellierung eines Shack-Hartmann-Wellenfrontsensors für dynamisch-optische Simulationen. Simtech-Projektarbeit SA-6 (Institut für Technische und Numerische Mechanik, Universität Stuttgart, 2014).
[2] R. Tyson, 'Principles of Adaptive Optics', 4th ed. (CRC Press, Boca Raton, 2015).
[3] M. Böhm, J.U. Pott, O. Sawodny, T. Herbst and M. Kürster, MNRAS Monthly Notices R. Astronom. Soc. 442, 2446–2455 (2014).
[4] T. Ruppel, S. Dong, F. Rooms, W. Osten and O. Sawodny, IEEE Trans. Control Syst. Technol. 21, 579–589 (2013).
[5] M. Böhm, J.U. Pott, O. Sawodny, D. Defrére and P. Hinz, IEEE Trans. Control Syst. Technol. 25, 1384–1393 (2016).
[6] J. Störkle and P. Eberhard, in 'Proc. SPIE, Integrated Modeling of Complex Optomechanical Systems II' (2016), vol. 10012, pp. 100120C–100120C–5.
[7] J. Störkle and P. Eberhard, in 'Proc. SPIE, Modeling, Systems Engineering, and Project Management for Astronomy VI' (2016), vol. 9911, pp. 99111E–99111E–15.
[8] J. Störkle, Dynamic simulation and control of optical systems. Dissertation, Schriften aus dem Institut für Technische und Numerische Mechanik der Universität Stuttgart, vol. 58 (Shaker Verlag, Aachen, 2018).
[9] J. Störkle and P. Eberhard, J. Astronom. Telescopes Instrum. Syst. (JATIS) 024001–1–024001–18 (2017).
[10] B. Abraham, S. Adkins, B. Alcott, D. Alvarez, R. Alvarez, et al., Thirty Meter Telescope — construction proposal. Technical Report (TMT Observatory Corporation, 2007).
[11] G. Ming Dai and V.N. Mahajan, J. Opt. Soc. Am. A 24, 139–155 (2007).
[12] J. Nijenhuis, R. Hamelinck and B. Braam, in 'Proc. SPIE, Modern Technologies in Space- and Ground-Based Telescopes and Instrumentation II' (2012), vol. 8450, pp. 84500A–84500A-9.

1 Find additional information on the software OM-Sim at http://www.itm.uni-stuttgart.de/research/omsim/omsim_en.php.